metals

MDPI

Article

Identification and Evolution of Intermetallic Compounds Formed at the Interface between In-48Sn and Cu during Liquid Soldering Reactions

Panju Shang [1], Feifei Tian [1,2] and Zhi-Quan Liu [1,3,*]

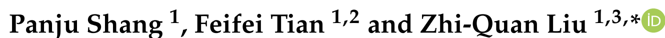

[1] Institute of Metal Research, Chinese Academy of Sciences, Shenyang 110016, China
[2] Nanjing Electronic Devices Institute, Nanjing 210016, China
[3] Shenzhen Institute of Advanced Technology, Chinese Academy of Sciences, Shenzhen 518055, China
* Correspondence: zqliu@siat.ac.cn

Abstract: It is difficult to confirm the existence of intermetallic compounds (IMCs) between SnIn and Cu, as their atomic numbers are very close, making it challenging to differentiate them through experimental tests. In order to determine IMCs and understand their growth mechanism, this study employed phase identification, morphology observation, and growth kinetics analyses on IMCs formed between In-48Sn solder and polycrystalline Cu substrate during liquid soldering. The experiments were conducted within a temperature range of 160~250 °C for up to 90 min. The obtained results indicated that IMCs formed at the interface depended strongly on the soldering temperature. During long-time soldering below 200 °C, one main IMC species, Cu_2(In,Sn), was found at the In-48Sn solder/Cu interface, which showed two different morphologies: a coarse-grained layer at the solder side and a fine-grained layer within the Cu component. When the soldering temperature was increased to 200 °C, $Cu_6(In,Sn)_5$ was the only intermetallic compound (IMC) that formed at the point where the In-48Sn/Cu eutectic interface existed. At 250 °C, with an increase in the soldering time, there was a formation of $Cu_9(In,Sn)_4$ between Cu and $Cu_6(In,Sn)_5$. The growth kinetics analyses indicated that the fast grain boundary/molten-channel diffusion of Cu into solder and their reaction with solder controlled the growth of the interfacial IMCs, with the activation energy of 24.56 kJ/mol when the sample was liquid-state-aged above 200 °C.

Keywords: In-48Sn solder alloy; Cu substrate; interfacial reaction; intermetallic compound; TEM

Citation: Shang, P.; Tian, F.; Liu, Z.-Q. Identification and Evolution of Intermetallic Compounds Formed at the Interface between In-48Sn and Cu during Liquid Soldering Reactions. *Metals* **2024**, *14*, 139. https://doi.org/10.3390/met14020139

Academic Editor: Jan Vrestal

Received: 25 December 2023
Revised: 15 January 2024
Accepted: 19 January 2024
Published: 23 January 2024

Copyright: © 2024 by the authors. Licensee MDPI, Basel, Switzerland. This article is an open access article distributed under the terms and conditions of the Creative Commons Attribution (CC BY) license (https://creativecommons.org/licenses/by/4.0/).

1. Introduction

It is an inevitable trend in the microelectronics industry to use lead-free solder as a substitute for lead-containing solder due to environmental and human health issues [1,2]. During the last decade, several kinds of lead-free solders have been developed. However, most of the current commercial lead-free solders, such as tin/silver (Sn/Ag) and tin/silver/copper (Sn/Ag/Cu), have higher melting temperatures (T_m of Sn/Ag and Sn/Ag/Cu are 217 and 221 °C, respectively) than that of the conventional tin–lead eutectic solder (183 °C) [3]. Thus, the reflow temperature during electronic assembly should be raised, which would result in larger thermal stresses generated by different thermal expansions between the device and the substrate, thereby leading to mechanical damage in the device. In view of this, low-melting-point solders were remarkable during soldering in reducing the thermal stresses [4]. Amongst the Pb-free alloy families, the In-48Sn eutectic alloy has attracted a great deal of attention because of its low melting temperature, higher ductility, better wettability, and longer fatigue life [5]. Studies have reported that In-Sn solders had been used for SMT applications, step soldering sequences, heat-sensitive devices, etc. [6–8].

Although several studies focused on the reaction between In-48Sn and Cu substrate, most of these works paid attention to relatively low reactive temperatures in order to

simulate the service conditions of solder joints. However, the findings reported in various studies were not entirely consistent with each other, especially regarding the identification of phases [9–15], which is essential to clarify the service reliability and failure mechanism of the solder joint. Roming et al. [9] conducted a two-step process where a Cu-based metal was dipped into molten solder. Subsequently, the samples were transferred to alumina boats and subjected to air aging at temperatures ranging from 60 °C to 110 °C. At the interface, two types of intermetallic compounds (IMCs), namely Cu_2(In,Sn) and Cu_2In_3Sn, were identified. Furthermore, their investigation revealed that the growth of Cu_2In_3Sn dominated the growth of the IMC layer (although the Cu_2(In,Sn) layer formed during dipping, it did not undergo any further growth). Vianco et al. [10] conducted a follow-up study in which copper was hot-dipped into a molten solder of 50In-50Sn and subsequently subjected to solid-state aging at temperatures of 75 °C, 80 °C, and 100 °C for up to 200 days. Their findings revealed that the IMC layer was composed of a thin layer of $Cu_{17}Sn_9In_{24}$ near the solder matrix and a thicker layer of $Cu_{26}Sn_{13}In_8$ on the side of the Cu substrate. Another study by Chuang et al. [11] reported that the likely phases at the interface after soldering the In-49Sn/Cu system at temperatures ranging from 60 °C to 110 °C were ε-Cu_3(In,Sn) and η-Cu_6(In,Sn)$_5$.

It is important to emphasize that all the aforementioned findings were acquired using either electron probe microanalysis (EPMA) or energy-dispersive X-ray spectroscopy (EDS) techniques. It is difficult to distinguish all of the IMCs formed between In-48Sn and Cu, such as Cu_6Sn_5, Cu_3Sn, Cu_7In_3, Cu_2In, Cu_9In_4, and $Cu_{11}In_9$ [16], limited by the resolution of EPMA or EDS. This means that only compositional information was not enough for phase identification. To provide a detailed proof for the identification of phases, specifically with regards to the crystallographic structure of IMCs, is imperative. In our recent work, TEM and precise electron diffraction techniques were used to conduct interfacial phase identification for our sample, which was reflowed at 160 °C for 5 s and then solid-state aged at 100 °C up to 7 days. The resulting IMC was identified as Cu_2(In,Sn) [17].

In recent years, the transient liquid phase (TLP) soldering process as a potential alternative method to improve the reliability of solder joints in electronic assemblies and systems operated at elevated temperatures has attracted much attention [18–20]. The transient liquid phase (TLP) soldering process involves melting a minor amount of metal, which helps to fill in any defects and enhance the strength of the joint. Additionally, by controlling the temperature distribution and using appropriate materials, this process can effectively prevent the occurrence of cracks. The TLP soldering process necessitates a soldering temperature that is higher than the melting point of the solder alloy. However, to prevent excessive evaporation or loss of the solder alloy, the temperature is typically maintained below 300 °C. As for Cu/In-48Sn/Cu solder joints, earlier work was performed by Sommadossi et al. as a diffusion-soldering process [21,22] and was primarily conducted from 180 to 400 °C. They reported two kinds of IMCs, Cu_2(In,Sn) and Cu_2In_3Sn, at the interface based on their EPMA data. In this study, we utilized transmission electron microscope observations and precise diffraction analysis to investigate interfacial evolutions between In-48Sn and Cu, offering a high-resolution approach for phase identification. Experiments were conducted over a temperature span of 160 °C to 250 °C, with a time limit of 90 min.

2. Experimental Procedure

2.1. Soldering Sample Preparation

In this study, oxygen-free high-conductivity (OFHC) multi-crystalline Cu samples were prepared by cutting them with spark erosion machining to dimensions of $10 \times 2.5 \times 2$ mm^3. The In-48Sn solder employed was fabricated by heating high-purity indium and tin until it became molten to produce a solid block of metal, which was subsequently subjected to cold-rolling to obtain a 1 mm thin sheet and cut into dimensions of 10×2.5 mm^2. To ready the Cu surfaces, they were ground and polished with 0.5 μm diamond paste, then cleansed in an ultrasonic bath of distilled water, containing acetone and methanol

alcohol. Afterwards, two copper sheets were bonded using eutectic SnIn solder to produce a sandwich comprising Cu-solder-Cu, with 50μm diameter brass wires inserted between them to control the thickness of the solder layer. The soldering process was performed for different durations ranging from 5 s to 90 min at varying temperatures, including 160 °C, 200 °C, 220 °C, and 250 °C.

2.2. Electron Microscopy Analysis

After the soldering process, the sample was cross-sectionally cut and subsequently polished using a BUEHLER polishing suspension (Bühler Group, Uzwil, Switzerland) that included 0.05 μm Al_2O_3 powder. The polishing process was conducted meticulously to ensure high-quality results. An etchant of 90% CH_3OH-10% HNO_3 was used to dissolve the remaining solder to observe the top view of the IMCs. Using an FEI Quanta 600 SEM (FEI company, Hillsboro, OR, USA) equipped with an Oxford Link ISIS EDS system (Oxford Instruments, Abingdon, UK), morphology observations were performed through scanning electron microscopy (SEM). To prepare the TEM foils, the slices underwent mechanical grinding until they reached a final thickness of 40 μm. They were then subjected to ion milling using a Gatan model 691 PIPS system (Gatan, Pleasanton, CA, USA) under conditions of 5.0 keV and 5 μA, with a low milling angle of less than 6°. Transmission electron microscopy (TEM) observations were conducted using FEI Tecnai F30 (FEI company, Hillsboro, OR, USA) and JEM-2100 electron microscopes (JEOL Ltd., Tokyo, Japan).

2.3. IMC Thickness Measurement

For the kinetic studies, the thickness of the IMC layer was digitally measured on SEM images using the following steps: (1) differentiate the individual IMC layers based on their image contrast using the commercial software "Adobe Photoshop"; (2) generate a binary image for the IMC layer and save it in BMP format; (3) utilize self-developed software to calculate the total area of the IMC layer, and subsequently divide the total area of the IMC layer by the length of the IMC layer to derive the mean thickness of each layer, even if the layer itself is non-uniform.

3. Experimental Results and Discussion

3.1. Interfacial IMC Evolution during Soldering at Different Temperatures

Figure 1 shows SEM images showing a cross-sectional view of the In-48Sn/Cu interface after soldering at 160 °C for different times. At the solder/Cu interface, only one kind of IMC layer could be distinguished by contrast analysis of the backscattering electron image in Figure 1. EDS analysis indicated that it consisted of 65.18 at.%Cu, 15.94 at.%In, and 18.88 at.%Sn, which corresponded to Cu-16In-19Sn. After soldering at 160 °C for 1 min, Figure 2 presents an interfacial TEM bright field (BF) image of the In-48Sn/Cu joint, along with the corresponding selected area electron diffraction patterns (SAEDPs). Detailed information of the interfacial microstructures indicated two different morphological IMC layers, as shown in Figure 2a. Upon examination, it was observed that an IMC layer exhibiting a fine-grained structure with a grain size of approximately 50 nm had formed at the Cu side of the joint. Conversely, at the solder side, the IMC grain size was much larger, at around 500 nm. In order to identify the crystallographic structure, the SAEDPs along the different zone axes were taken when the specimen was rotated in TEM. Figure 2b,c is from grain A in Figure 2a, which represents the grains in the coarse-grained IMC layer, and Figure 2d,e is from grain B in Figure 2a, which represents the grains in the fine-grained IMC layer. The lattice parameters for hexagonal Cu_2In, with dimensions of a = b = 0.4292 nm, c = 0.5232 nm, $\alpha = \beta = 90°$, and $\gamma = 120°$ [23], were utilized for indexing and assigning crystallographic parameters to the SAEDPs along the $[01\bar{1}1]$ zone axis and $[14\bar{5}3]$ zone axis in Figure 2b,c, respectively. Similarly, the $[11\bar{2}0]$ zone axis and $[02\bar{2}1]$ zone axis were employed to index the SAEDPs in Figure 2d,e, respectively. This indicates a consistent match between the

observed diffraction patterns and the hexagonal Cu_2In crystal structure. The angle of rotation from the zone axis A to zone axis B can be calculated by the following equation:

$$\cos\theta = \cos(Y_1 - Y_2)\cos(X_1 - X_2) \quad (1)$$

where θ is the angle of rotation from zone axis A to zone axis B, (X_1, Y_1) is the rotation angle along the x, y axis when the electron beam is parallel to zone axis A, and (X_2, Y_2) is the rotation angle along the x, y axis when the electron beam is parallel to zone axis B. Based on Equation (1), the experimental measurement of the angle of rotation from the $[14\bar{5}3]$ zone axis to the $[01\bar{1}1]$ zone axis was found to be 14.27°, which is in close agreement with the theoretical value of 14.02°. Similarly, the experimental measurement of the rotational deviation from the $[11\bar{2}0]$ zone axis to the $[02\bar{2}1]$ zone axis was 36.39°, while the theoretical angle was 35.22°. Based on the morphologies of the IMC layers in Figure 2a, it can be observed that they are different. The black arrowheads indicate the interface between IMC and Cu substrate, while the white arrowheads show the interface between coarse IMC grains and fine IMC grains. However, both IMC layers belong to the Cu_2In type. It is important to note that during soldering, some Sn atoms merged with the Cu_2In lattice and occupied the substitutional sites of the In atoms due to the similar atomic diameters of In and Sn. Therefore, the intermetallic compound found at the interface is consistent with the hexagonally structured Cu_2(In,Sn) phase.

When the soldering temperature was raised up to 200 °C, the interfacial IMC phase changed simultaneously. Moreover, with the increase in soldering time, IMC increasingly depleted from the solder/IMC interface into the bulk solder, as shown with short arrowheads in Figure 3. The EDS analysis for the interfacial IMC layer (marked with long arrows near interface) indicated that it consisted of 56.90 at.% Cu, 19.86 at.% In, and 23.24 at.% Sn, which corresponded to Cu-19In-23Sn. The interfacial microstructure of the In-48Sn/Cu contact region and the associated SAEDPs were observed after polishing and soldering at a temperature of 200 °C for a period of 10 min in Figure 4. The SAEDPs illustrated in Figure 4b,c were identified according to the crystalline framework of Cu_6Sn_5, which is characterized by a monoclinic lattice characterized by dimensions of a = 1.103 nm, b = 0.7294 nm, c = 0.983 nm, and β = 98.82° [24]. During the experimental process, the rotation angle from the zone axis $[\bar{2}51]$ to the zone axis $[\bar{3}54]$ yielded a measured value of 26.2°, which was consistent with the theoretical value of 26.63°. Hence, it can be concluded that the IMC present at the interface can be identified as Cu_6(In,Sn)$_5$.

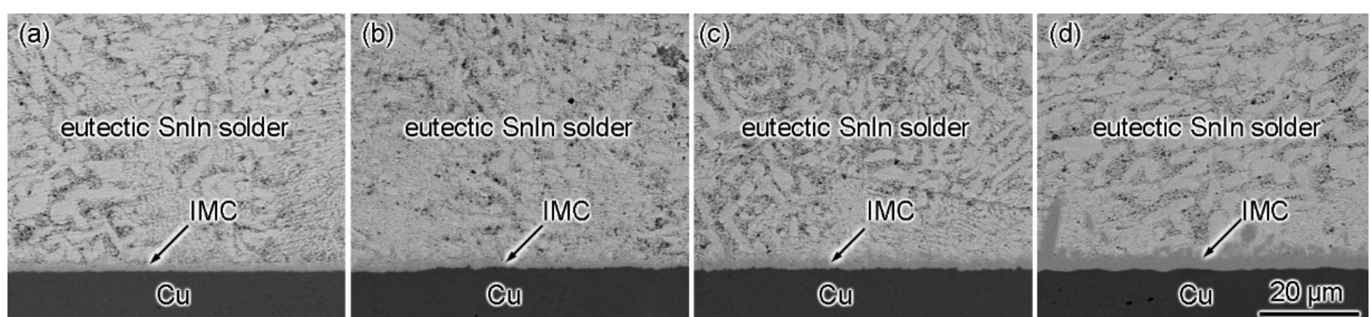

Figure 1. SEM images showing interfacial microstructures of In-48Sn/Cu interface after liquid-state aging for different times at 160 °C: (**a**) 5 min; (**b**) 10 min; (**c**) 30 min; (**d**) 60 min.

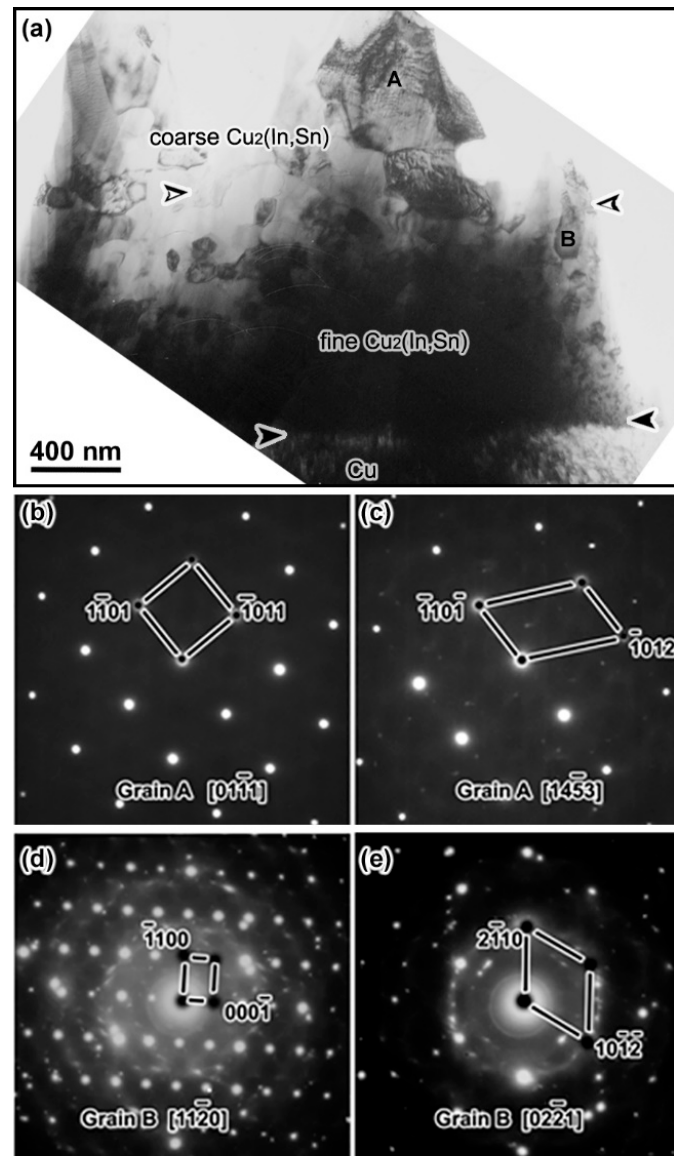

Figure 2. TEM bright field image (**a**) showing interfacial microstructures of In-48Sn/Cu interface after reflowing at 160 °C for 1 min, and the corresponding SAEDPs of (**b**,**c**) from grain A in (**a**), as well as SAEDPs of (**d**,**e**) from grain B in (**a**).

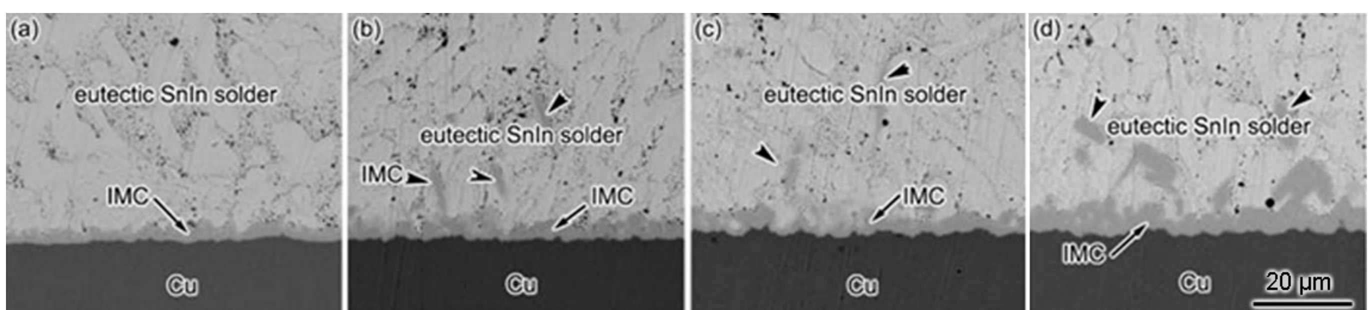

Figure 3. SEM images showing interfacial microstructures of In-48Sn/Cu interface after liquid-state aging for different times at 200 °C: (**a**) 5 min; (**b**) 10 min; (**c**) 30 min; (**d**) 60 min. Long arrows represent the IMCs at the interface after reaction, while short arrowheads indicate the depleted IMCs inside the bulk solder.

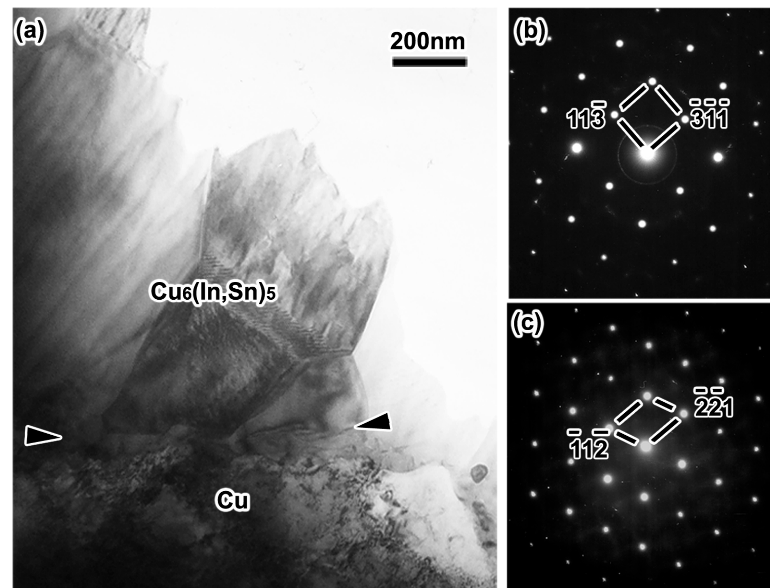

Figure 4. TEM bright field image (**a**) of In-42Sn/Cu interface after liquid-state aging for 10 min at 200 °C and corresponding SAEDPs (**b**,**c**).

Figure 5 shows the SEM cross-sectional morphologies of the In-48Sn/Cu interface after soldering at 250 °C for different times. Observably, the IMC thickness on the solder side exhibited an increase with the gradual soldering time. Additionally, at the solder/IMC interface, there was a noticeable depletion of IMC from the IMC layer into the solder, consistent with the phenomenon observed in Figure 3. It is widely believed that the quantity of IMC depleted into solder from the solder/IMC interface is related to the soldering temperature. In addition, the higher soldering temperature required a shorter aging time when the IMC at the solder/IMC interface started to deplete into the solder. The IMC layer formed at the solder side dominates the growth of the whole IMC layers. The EDS analysis revealed that it was composed of 57.27 at.%Cu, 21.06 at.%In, and 21.67 at.%Sn. This is close to the elemental composition of $Cu_6(In,Sn)_5$, which is verified by the TEM BF image and precise electron diffraction analyses. At the Cu side, with a rise in the liquid-reaction temperature, a new IMC appeared between the $Cu_6(In,Sn)_5$ and Cu substrate. Different imaging contrasts indicated the different types of IMCs formed at the In-48Sn/Cu interface, which are shown by arrows in Figure 5. It can be seen that the IMC layer is thin and grows slowly during subsequent liquid-state aging. The EDS analysis indicated that it consisted of 73.89 at.%Cu, 12.17 at.%In, and 13.94 at.%Sn. However, it was not adequate to identify the phase crystal structure because of the similar elemental compositions of Cu_7In_3, Cu_9In_4, and Cu_2In. Further investigation was needed. Figure 6 shows a bright field image of the In-48Sn/Cu interface and SAEDPs of the IMC at the Cu side. The SAEDPs were identified as having a Cu_9In_4-type crystal structure, which exhibits a cubic lattice with dimensions of a = b = c = 0.9097 nm and angles of $\alpha = \beta = \gamma = 90°$ [23]. The rotation angle values measured in the experiment and the theoretical values are listed in Table 1. It is evident that the rotation angle values measured in the experiment are close to the theoretical values. Hence, the intermetallic compound generated at the Cu interface region between In-48Sn and Cu can be characterized as $Cu_9(In,Sn)_4$, whose crystal structure belongs to the Cu_9In_4 phase.

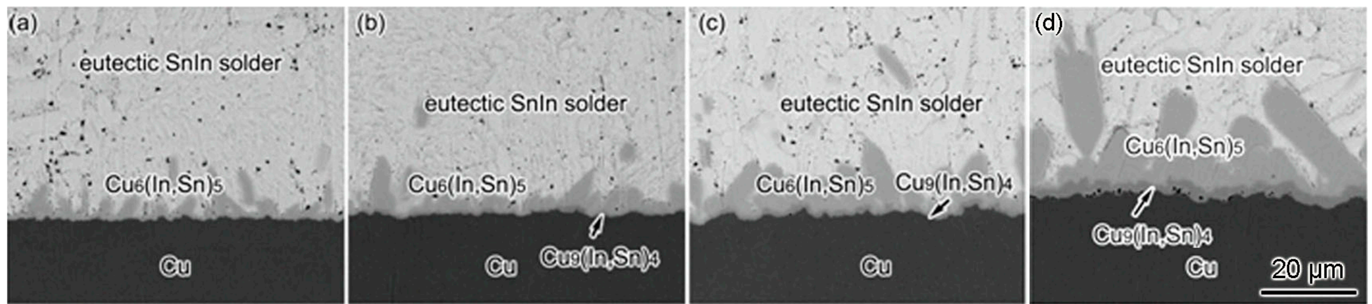

Figure 5. SEM images showing interfacial microstructures of In-48Sn/Cu interface after liquid-state aging for different times at 250 °C: (**a**) 5 min; (**b**) 10 min; (**c**) 30 min; (**d**) 60 min.

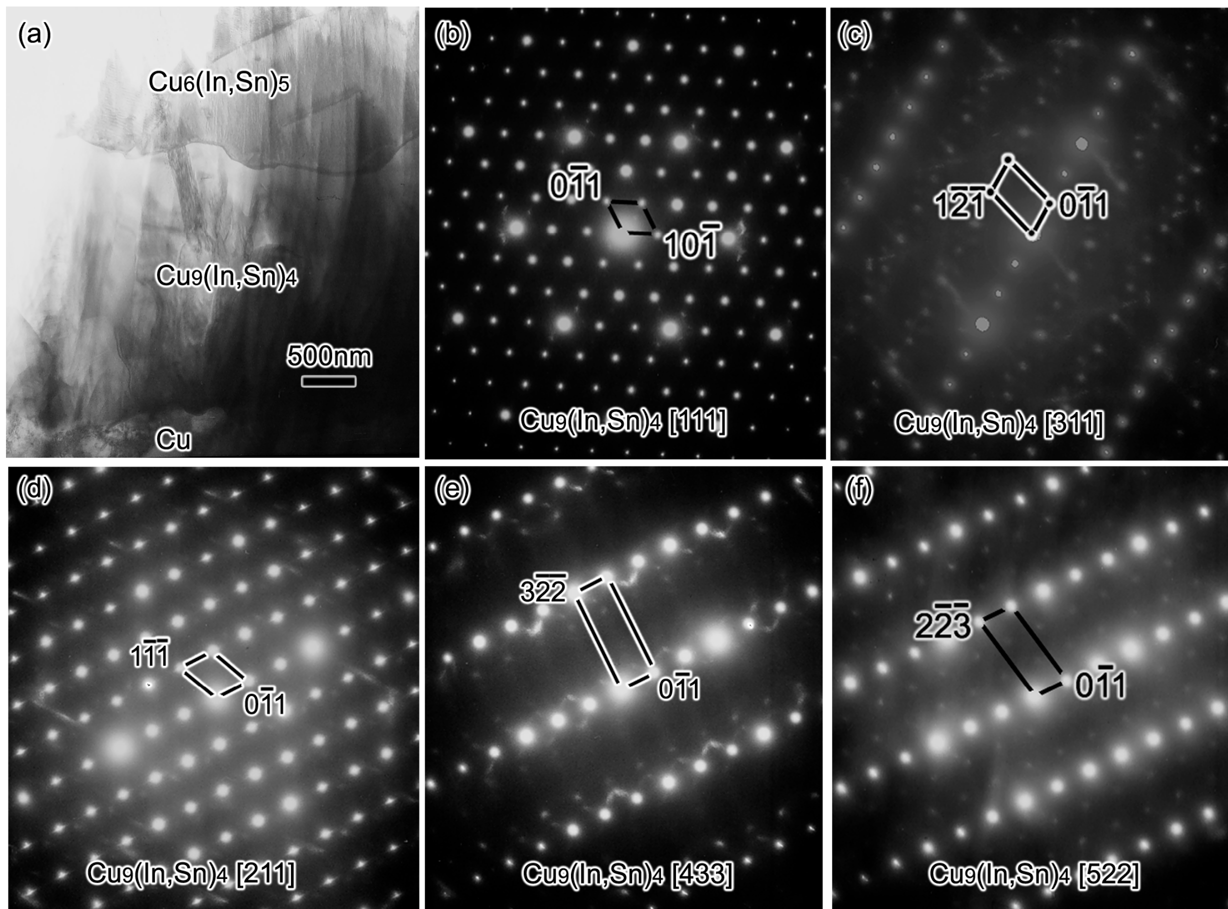

Figure 6. TEM bright field image showing the interfacial microstructure between eutectic SnIn and Cu (**a**) and SAEDPs (**b**–**f**) of interfacial IMC beside the Cu substrate after liquid-state aging at 250 °C for 30 min.

Table 1. A comparison of the rotation angle measured in the experiment with the theoretical values.

Zone Axis 1	Zone Axis 2	Experimental Values (°)	Theoretical Values (°)
[311]	[111]	29.50	28.78
[211]	[433]	11.42	11.72
[433]	[522]	17.19	16.29

According to the above mentioned results, the microstructures and crystallographic structure of interfacial IMCs were obviously affected by the soldering temperature. Numer-

ous theoretical and experimental studies have been conducted to establish the complete ternary phase diagram of Cu-In-Sn [25,26]. Figure 7a displays the isothermal section of the Cu-In-Sn ternary phase diagram at 110 °C, as presented by Liu et al., which is the lowest temperature reported in the literature for this ternary system [25]. They identified the η phase, which corresponds to Cu_6Sn_5 or Cu_2In, as continuously existing from the Cu-In to the Cu-Sn systems [27]. However, when compared to the findings of the current study, it appears that the compositional range of the η phase should be broader. This observation was also supported by Lin et al. [26], who investigated the isothermal section of the Cu-In-Sn ternary phase diagram at 250 °C. They observed that the η-(Cu_6Sn_5, Cu_2In) phase formed a continuous solid solution, as depicted in Figure 7b. These studies indicate that the understanding of the η phase in the Cu-In-Sn system has evolved with further investigations, suggesting a wider compositional range for this phase than previously reported. Indeed, the crystal structures between Cu_6Sn_5 and Cu_2In are difficult to distinguish based solely on these studies. The η-Cu_6Sn_5 phase is known to possess a NiAs B8 crystal structure with lattice parameters a = b = 0.4200 nm, c = 0.5090 nm, $\alpha = \beta = 90°$, and $\gamma = 120°$, which is stable above 189 °C [28,29]. It is important to mention that η-Cu_6Sn_5 often displays a superstructure phenomenon [30,31]. This superstructure refers to a crystalline formation that transitions from disorder to orderliness when the alloy cools slowly. Additionally, the superstructure enhances the high-temperature stability and reduces resistance in the crystalline structure. Based on the detailed electron diffraction patterns (EDPs) depicted in Figure 4b,c, none of the three-modulated or five-modulated structures were observed. When the temperature is below 189 °C, Cu_6Sn_5 transforms into η′-Cu_6Sn_5, which possesses a monoclinic structure with lattice parameters a = 1.1033 nm, b = 0.7294 nm, c = 0.9830 nm, $\alpha = 90°$, $\beta = 98.82°$, and $\gamma = 90°$ [28]. It is evident that the lattice parameters of η′-Cu_6Sn_5 were not consistent with the observed EDPs when the In-48Sn/Cu joint was soldered below 160 °C (although this soldering temperature could be improved to 180 °C), as depicted in Figure 2b,d. Based on the factors mentioned above, including the similar diameters of Sn and In atoms, it can be inferred that the IMC that was formed at the interface between the eutectic SnIn solder and Cu during the process soldering below 180 °C may be identified as a hexagonal Cu_2In lattice that has been dissolved with some Sn atoms. However, the crystal structure of IMC formed above 200 °C should be identified as $Cu_6(In,Sn)_5$, as shown in Figures 3 and 4.

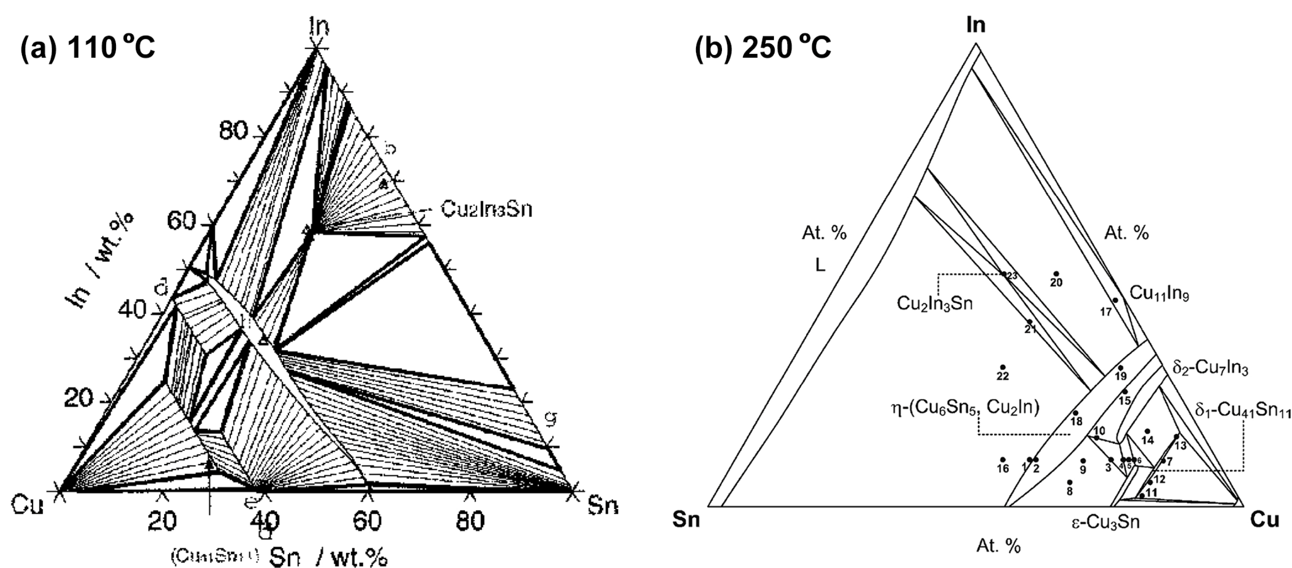

Figure 7. Ternary Cu-In-Sn isothermal section at 110 °C (adapted from Ref. [25]) and 250 °C (adapted from Ref. [26]).

Although the $Cu_9(In,Sn)_4$ phase was not discovered in the ternary phase diagram of Liu et al. [25] and Lin et al. [26], it was universally observed in the Cu/In thin films [12,13] when the soldering temperature increased above 200 °C. Thus, during liquid-state aging, the $Cu_6(In,Sn)_5$ phase first nucleated and grew at the interface of the liquid solder/Cu substrate [32]. It is known that the melting point of the $Cu_6(In,Sn)_5$ phase is higher than the soldering temperature (250 °C). Thus, the formation of the $Cu_9(In,Sn)_4$ phase is believed to be a solid–solid diffusion process, which means that Cu further reacts with the $Cu_6(In,Sn)_5$ phase to form the $Cu_9(In,Sn)_4$ phase [33]. In summary, the species of interfacial IMCs formed at the In-48Sn/Cu interface had a close relationship with the soldering temperature and are listed in Table 2.

Table 2. The IMC species formed at the In-48Sn/Cu interface during long-time liquid soldering ranging from 160 °C to 250 °C.

	Soldering Temperature (°C)		
	160	**200**	**250**
IMC	Duplex $Cu_2(In,Sn)$	$Cu_6(In,Sn)_5$	$Cu_6(In,Sn)_5$ + $Cu_9(In,Sn)_4$

3.2. Growth Kinetics of the Interfacial IMC Layer

Generally, the growth of the IMC layer may be expressed as a function of aging time as:

$$\Delta x = kt^n \text{ or } \log \Delta x = A + n \log t \quad (2)$$

where Δx is the IMC thickness, k—the growth rate constant, t—the reaction time, and n is the time exponent. There is an empirical notion that the values of n could reflect the rate-controlling mechanisms of IMC growth. Generally, n takes the value of 0.5 when IMC growth is controlled by volume diffusion. In contrast, if n takes the value of 1, it means that the growth of IMC is controlled by the reaction at the interface.

Figure 8 shows the growth kinetics results after the samples were liquid-state soldered at 200, 220, and 250 °C. The value of the time exponent (n) can be obtained from the slope of $\log \Delta x$ versus $\log t$, which is listed in Table 3 with the growth rate constants at different aging temperatures. From Table 3, it was observed that IMC growth was preferably controlled by species diffusion during liquid-state soldering at the temperature range of the present study, although the time exponent (n) was not exactly 0.5.

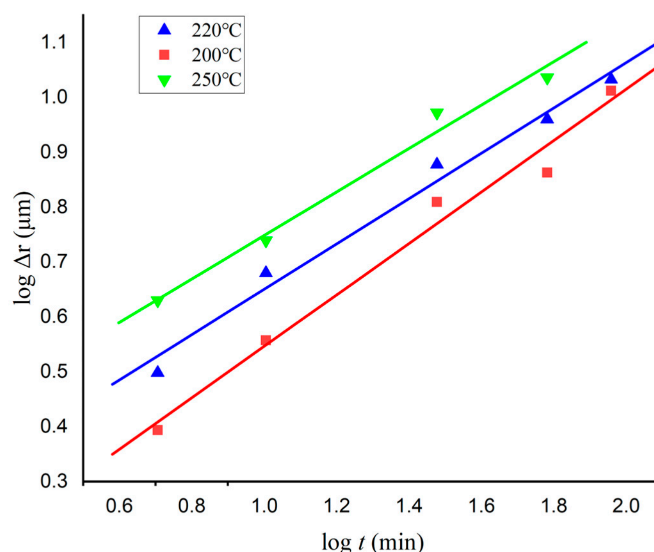

Figure 8. The logarithm of IMC thickness as a function of the logarithm of aging time during liquid-state aging at a temperature range of 200 °C to 250 °C.

Table 3. Growth rate exponents *n* obtained from Equation (2) when the samples were soldered at a temperature range of 200 °C to 250 °C.

	Soldering Temperature (°C)		
	200	220	250
n	0.498	0.440	0.447

An Arrhenius relationship was used to calculate the activation energy for IMC growth, as follows:

$$k = k_0 \exp(-\frac{Q}{RT}) \quad (3)$$

where k is the growth rate constant, k_0 is the pre-exponential coefficient, Q is activation energy, R is the gas constant (8.314 J/mol K), and T is the aging temperature (absolute units). The activation energy for the interfacial IMC growth during liquid-state soldering, obtained from the slope of the Arrhenius plots, as shown in Figure 9, is 24.56 kJ/mol, which is distinctly smaller than the activation energy of scallop-type Cu_6Sn_5, where the activation energy was around 52.48 kJmol^{-1} [34]. However, it is consistent with the activation energy of Cu in liquid Sn (19.5 kJmol^{-1}) [35]. Figure 10 shows top-viewed images of IMC morphology for In-48Sn/Cu soldered under various soldering conditions. It can be seen that three types of $Cu_6(In,Sn)_5$ morphology were observed in the In-48Sn/Cu interface during soldering. In detail, only needle-like $Cu_6(In,Sn)_5$ formed at the shorter soldering time, as shown in Figure 10a,e. With an extension in soldering time, the needle-like $Cu_6(In,Sn)_5$ transformed into rod-like $Cu_6(In,Sn)_5$ of polyhedron-type [36]. Finally, the IMC changed to a tube-like morphology with a core, as shown in Figure 10d. Whatever the morphology of the $Cu_6(In,Sn)_5$ IMC, a ubiquitous phenomenon is that there are grain boundaries/molten channels in between $Cu_6(In,Sn)_5$ crystals, which could be fast diffusion channels of Cu to solder [37,38]. This is different from Sn diffusion along the grain boundary/molten channel controlled by the growth of Cu_6Sn_5 [37]; otherwise, the morphology of $Cu_6(In,Sn)_5$ would be scalloped-type and the time exponent (n) of the IMC growth kinetic would be 1. Therefore, during soldering above 200 °C, Cu diffusing along the grain boundary/molten channel in between $Cu_6(In,Sn)_5$ crystals controlled IMC growth.

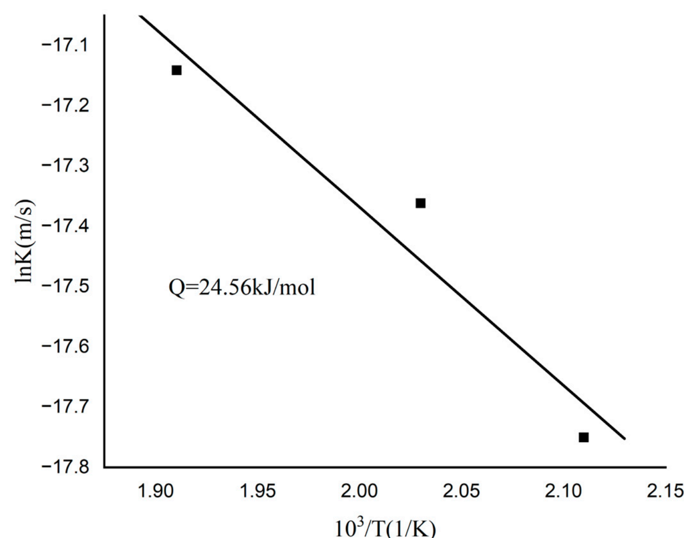

Figure 9. An Arrhenius plot for the IMC layer formed during eutectic SnIn/Cu soldering reactions at the temperature range of 200 °C to 250 °C.

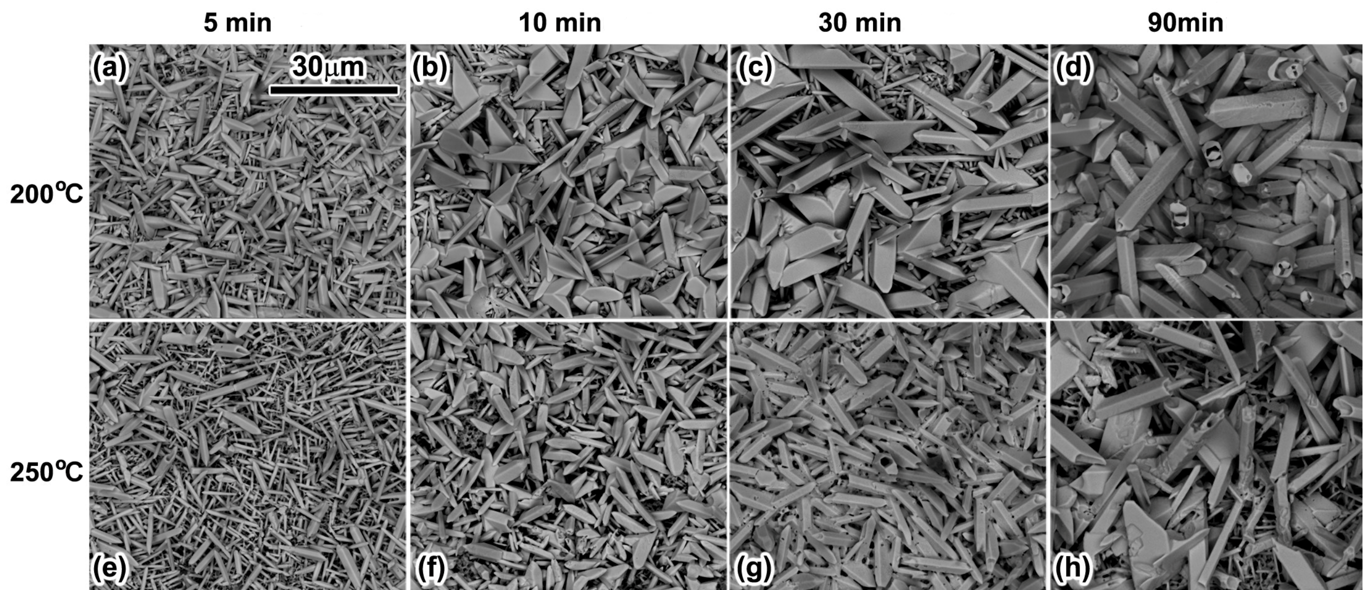

Figure 10. Top-viewed images of IMC morphology for 48Sn52In/Cu soldered at 200 °C for (**a**) 5 min, (**b**) 10 min, (**c**) 30 min and (**d**) 90 min, together with those soldered at 250 °C for (**e**) 5 min, (**f**) 10 min, (**g**) 30 min and (**h**) 90 min. The scale bar in (**a**) is applicable for all images.

4. Conclusions

Microstructural changes between In-48Sn and Cu were investigated using TEM bright-field (BF) imaging and precise diffraction analyses over a temperature range of 160 °C to 250 °C for up to 90 min. When the sample was subjected to reflow at 160 °C for an extended period, only one type of intermetallic compound (IMC) formed at the interface between In-48Sn and Cu, which was Cu_2(In,Sn). However, two distinct morphologies were observed: a coarse-grained layer on the solder side and a fine-grained layer on the Cu side. Precise electron diffraction analyses revealed that both IMC layers exhibited a Cu_2In-type crystal structure. As the aging temperature increased beyond 200 °C, a phase called Cu_6(In,Sn)$_5$ initially nucleated and grew at the interface between In-48Sn and Cu. Subsequently, a Cu_9(In,Sn)$_4$ phase formed through a solid-state reaction between Cu_6(In,Sn)$_5$ and Cu. Growth kinetic analyses indicated that the activation energy of IMC growth is 24.56 kJ/mol, which is consistent with the activation energy of Cu in liquid Sn (19.5 kJ/mol). This implied that the IMC growth above 200 °C was mainly controlled by the diffusion of Cu atoms dissolved into the liquid solder through grain boundaries/molten channels in between Cu_6(In,Sn)$_5$ crystals.

Author Contributions: Conceptualization, Z.-Q.L.; methodology, P.S.; formal analysis, P.S., F.T. and Z.-Q.L.; investigation, P.S. and F.T.; writing—original draft preparation, P.S.; writing—review and editing, F.T. and Z.-Q.L.; visualization, P.S. and F.T.; supervision, Z.-Q.L.; funding acquisition, Z.-Q.L. All authors have read and agreed to the published version of the manuscript.

Funding: This work was partially supported by the Guangdong Basic and Applied Basic Research Foundation (Grant No. 2022B1515120037) and Shenzhen Science and Technology Program (Grant No. KJZD20230923112800002).

Data Availability Statement: The data presented in this study are available on request from the corresponding author. The data are not publicly available due to privacy.

Acknowledgments: The authors would like to thank WenJie Li for his help on the data analysis and manuscript editing.

Conflicts of Interest: Author Feifei Tian was employed by the Nanjing Electronic Devices Institute. The remaining authors declare that the research was conducted in the absence of any commercial or financial relationships that could be construed as a potential conflict of interest.

References

1. Abtew, M.; Selvaduray, G. Lead-free solders in microelectronics. *Mater. Sci. Eng. R* **2000**, *27*, 95–141. [CrossRef]
2. Li, D.; Liu, C.; Conway, P.P. Characteristics of intermetallics and micromechanical properties during thermal ageing of Sn–Ag–Cu flip-chip solder interconnects. *Mater. Sci. Eng. A* **2005**, *391*, 95–103. [CrossRef]
3. Li, Y.; Wong, C.P. Recent advances of conductive adhesives as a lead-free alternative in electronic packaging: Materials, processing, reliability and applications. *Mater. Sci. Eng. R* **2006**, *51*, 1–35. [CrossRef]
4. Liu, Y.; Tu, K.N. Low melting point solders based on Sn, Bi, and In elements. *Mater. Today Adv.* **2020**, *8*, 100115. [CrossRef]
5. Kim, D.G.; Jung, S.B. Interfacial reactions and growth kinetics for intermetallic compound layer between In–48Sn solder and bare Cu substrate. *J. Alloys Compd.* **2005**, *386*, 151–156. [CrossRef]
6. Mei, Z.; Morris, J.W. Characterization of eutectic Sn-Bi solder joints. *J. Electron. Mater.* **1992**, *21*, 599–607. [CrossRef]
7. Huang, C.Y.; Chen, S.W. Interfacial reactions in In-Sn/Ni couples and phase equilibria of the In-Sn-Ni system. *J. Electron. Mater.* **2002**, *31*, 152–160. [CrossRef]
8. Zhou, J.; Tan, X.F.; McDonald, S.D.; Nogita, K. Mechanical Properties and Microstructure of Binary In-Sn Alloys for Flexible Low Temperature Electronic Joints. *Materials* **2022**, *15*, 8321. [CrossRef]
9. Romig, A.D., Jr.; Yost, F.G. *Proceedings Conference Microbeam Analysis*; San Francisco Press: San Franciso, CA, USA, 1984; pp. 87–92.
10. Vianco, P.T.; Hlava, P.F.; Kilgo, A.C. Intermetallic compound layer formation between copper and hot-dipped 100In, 50In-50Sn, 100Sn, and 63Sn-37Pb coatings. *J. Electron. Mater.* **1994**, *23*, 583–594. [CrossRef]
11. Chuang, T.H.; Chang, S.Y.; Tsao, L.C.; Weng, W.P.; Wu, H.M. Intermetallic compounds formed during the reflow of In-49Sn solder ball-grid array packages. *J. Electron. Mater.* **2003**, *32*, 195–200. [CrossRef]
12. Roy, R.; Sen, S.K.; Sen, S. The formation of intermetallics in Cu/In thin films. *J. Mater. Res.* **1992**, *7*, 1376–1386. [CrossRef]
13. Roy, R.; Pradhan, S.K.; De, M.; Sen, S.K. Structural characterization of the CuIn intermetallic phase produced by interfacial reactions in Cu/In bimetallic films. *Thin Solid Films* **1993**, *229*, 140–142. [CrossRef]
14. Sommadossi, S.; Huici, J.; Khanna, P.K.; Gust, W.; Mittemeijer, E.J. Mechanical properties of Cu/In–48 Sn/Cu diffusion-soldered joints. *Int. J. Mater. Res.* **2002**, *93*, 496–501. [CrossRef]
15. Wu, H.F.; Chiang, M.J.; Chuang, T.H. Selective formation of intermetallic compounds in Sn-20In-0.8 Cu ball grid array solder joints with Au/Ni surface finishes. *J. Electron. Mater.* **2004**, *33*, 940–947. [CrossRef]
16. Subramanian, K.N.; Chen, S.W.; Wang, C.H.; Lin, S.K.; Chiu, C.N. Phase diagrams of Pb-free solders and their related materials systems. *J. Mater. Sci. Mater. Electron.* **2007**, *18*, 19–37.
17. Shang, P.J.; Liu, Z.Q.; Li, D.X.; Shang, J.K. Intermetallic compound identification and Kirkendall void formation in eutectic SnIn/Cu solder joint during solid-state aging. *Philos. Mag. Lett.* **2011**, *91*, 410–417. [CrossRef]
18. Pawar, K.; Dixit, P. Investigation of Cu-Sn-Cu transient liquid phase bonding for microsystems packaging. *Mater. Manuf. Process.* **2023**, *38*, 284–294. [CrossRef]
19. Wang, X.; Zhang, L.; Chen, C.; Lu, X. Effect of AlN on the microstructure evolution of Cu/Sn58Bi/Cu solder joints for 3D packaging at different bonding times. *J. Mater.* **2023**, *25*, 4488–4496. [CrossRef]
20. Yang, L.; Yang, Y.; Zhang, Y.; Xu, F.; Qiao, J.; Lu, W.; Yu, B. Microstructure evolution and mechanical properties of the In–Sn–20Cu composite particles TLP bonding solder joints. *Appl. Phys.* **2020**, *126*, 343. [CrossRef]
21. Sommadossi, S.; Gust, W.; Mittemeijer, E.J. Characterization of the reaction process in diffusion-soldered Cu/In–48 at.% Sn/Cu joints. *Mater. Chem. Phys.* **2003**, *77*, 924–929. [CrossRef]
22. Sommadossi, S.; Guillermet, A.F. Interface reaction systematics in the Cu/In–48Sn/Cu system bonded by diffusion soldering. *Intermetallics* **2007**, *15*, 912–917. [CrossRef]
23. Che, G.C.; Ellner, M. Powder crystal data for the high-temperature phases Cu_4In, Cu_9In_4(h) and Cu_2In(h). *Powder Diffr.* **1992**, *7*, 107–108. [CrossRef]
24. Burkhardt, W.; Schubert, K. Über messingartige Phasen mit A3-verwandter Struktur. *Int. J. Mater. Res.* **1959**, *50*, 442–452. [CrossRef]
25. Liu, X.J.; Liu, H.S.; Ohnuma, I.; Kainuma, R.; Ishida, K.; Itabashi, S.; Yamaguchi, K. Experimental determination and thermodynamic calculation of the phase equilibria in the Cu-In-Sn system. *J. Electron. Mater.* **2001**, *30*, 1093–1103. [CrossRef]
26. Lin, S.K.; Chung, T.Y.; Chen, S.W.; Chang, C.H. 250° C isothermal section of ternary Sn-In-Cu phase equilibria. *J. Mater. Res.* **2009**, *24*, 2628–2637. [CrossRef]
27. Tian, F.F.; Pang, X.Y.; Xu, B.; Liu, Z.Q. Evolution and growth mechanism of Cu_2(In,Sn) formed between In-48Sn solder and polycrystalline Cu during long-time liquid-state aging. *J. Electron. Mater.* **2020**, *49*, 2651–2659. [CrossRef]
28. Larsson, A.K.; Stenberg, L.; Lidin, S. The superstructure of domain-twinned η'-Cu_6Sn_5. *Acta Crystall.* **1994**, *50*, 636–643. [CrossRef]
29. Larsson, A.K.; Stenberg, L.; Lidin, S. Crystal structure modulations in η-Cu_5Sn_4. *Z. Krist.* **1995**, *210*, 832–837. [CrossRef]
30. Christy, A.G.; Larsson, A.K. Computer Simulation of Modulated Structures and Diffuse Scattering inB8-type (Co, Ni, Cu)$_{1+x}$(Ge, Sn) Phases. *J. Solid State Chem.* **1998**, *135*, 269–281. [CrossRef]
31. Du, Y.; Qiao, Y.; Ren, X.; Lai, Y.; Zhao, N. Characterization of Sn-xIn Solders and Thermomigration-Induced Interfacial IMC Growth of Cu/Sn-xIn/Cu Micro Solder Joints. *Electronics* **2023**, *12*, 1899. [CrossRef]
32. Chang, F.L.; Lin, Y.H.; Hung, H.T.; Kao, C.W.; Kao, C.R. Artifact-Free Microstructures in the Interfacial Reaction between Eutectic In-48Sn and Cu Using Ion Milling. *Materials* **2023**, *16*, 3290. [CrossRef] [PubMed]

33. Tian, F.F.; Li, C.F.; Zhou, M.; Liu, Z.Q. The interfacial reaction between In-48Sn solder and polycrystalline Cu substrate during solid state aging. *J. Alloys Compd.* **2018**, *740*, 500–509. [CrossRef]
34. Suh, M.S.; Park, C.J.; Kwon, H.S. Growth kinetics of Cu–Sn intermetallic compounds at the interface of a Cu substrate and 42Sn–58Bi electrodeposits, and the influence of the intermetallic compounds on the shear resistance of solder joints. *Mater. Chem. Phys.* **2008**, *110*, 95–99. [CrossRef]
35. Ma, C.H.; Swalin, R.A. A study of solute diffusion in liquid tin. *Acta Metall.* **1960**, *8*, 388–395. [CrossRef]
36. Liu, Z.; Yang, L.; Lu, K.J.; Zhang, Y.C.; Xu, Y.H.; Xu, F.; Gao, H.M. IMC growth and mechanical properties of Cu/In-48Sn/Cu solder joints. *J. Electron. Mater.* **2021**, *50*, 3326–3333. [CrossRef]
37. Schaefer, M.; Fournelle, R.A.; Liang, J. Theory for intermetallic phase growth between Cu and liquid Sn-Pb solder based on grain boundary diffusion control. *J. Electron. Mater.* **1998**, *27*, 1167–1176. [CrossRef]
38. Wang, J.; Mao, D.; Shi, L.; Zhang, W.; Zhang, X. Effect of Zinc Addition on the Microstructure, Thermal and Mechanical Properties of Indium-Ti$_{n-x}$ Zinc Alloys. *J. Electron. Mater.* **2019**, *48*, 817–826. [CrossRef]

Disclaimer/Publisher's Note: The statements, opinions and data contained in all publications are solely those of the individual author(s) and contributor(s) and not of MDPI and/or the editor(s). MDPI and/or the editor(s) disclaim responsibility for any injury to people or property resulting from any ideas, methods, instructions or products referred to in the content.